SPIRE
Sustainable Process Industry through Resource and Energy Efficiency

DISIRE

Grant agreement no.	**636834**
Project acronym	**DISIRE**
Project full title	**Integrated Process Control Based on Distributed In-Situ Sensors into Raw Materials and Energy**
Dissemination level	PU
Date of Delivery	30/10/15
Deliverable Number	D3.1
Deliverable Name	Sensor technology selection report
AL / Task related	T3.1
Author	J. Johansson (LTU), J. Borg (LTU), I. M.Cassissa (D'Appolonia)
Contributors	LTU, LKAB, KGHM, WUT, IMTL, CUP, ETEC, CIRC, DCI, DAPP, MEFOS
Keywords:	Sensor selection, process parameter
Abstract	This report presents sensor technology and related technical challenge divided into three main sensor areas: hot side wireless sensors, cold side wireless sensors, and fiber optical sensors. For each sensor area, the report identifies concerned processes and parameters, lists possible sensor solutions, and in detail discusses related technical challenges and ongoing work. The hot side wireless sensors will focus on measurements of temperature and oxygen content. A major challenge is thermal insulation and time of survival in the extreme environments. Here, viable solutions for life lengths of 20-30 minutes for small (8 cm) devices have been found. Furthermore, the radio environment in the hot side is unknown and will be further researched. The cold side wireless sensors will concentrate on positioning. This will be achieved through passive RFID in the transportation chain, and through 3-dimensional signal strength or time-of-flight solutions in storage areas. Also here, the radio environment is a challenge. In order to better handle this, technical development focuses on the implementation of solutions using the 13.56 MHz frequency band. The fiber optic sensors will be used to measure process temperatures in areas with relatively low ($< 300^\circ$ C) temperatures. Concerned process sections include the LPG header in the cracking furnace, temperature across the naphtha header and temperature profile of the primary fractionators distillation column. Challenges regarding fiber optic sensors include resistance to higher temperatures and cost picture.

Contents

List of Figures

List of Tables

1 Introduction

This report presents the current status of the selection of sensors to be developed and applied within WP3. One major input to this report is the work performed in WP1 and presented in D1.2. Therein, the four main processes are presented, and their requirements on sensing are listed. On the contrary to D1.2, the structure for this report is based on the technologies of sensors and the requirements thereon, rather than on again listing the processes. Nevertheless, emphasis is made to clarify in the discussions on sensor technologies towards which process they are aiming.

For the work in DISIRE, the selection of what sensor to use is not the only challenge. The environments in where the senors will be used are hostile, and the implementation of the sensor in the speciifc environment is a major challenge. Thus, in addition to sensor presentation, this report also describes major parts of the underlying work that has, and will be, performed in order to facilitate the use of the sensors in their intended environments.

2 Hot side wireless sensors

In the writing of the DISIRE project it was envisaged that wireless sensors were to be developed and deployed mainly on the cold side of processes. However, as the project has progressed, it has become clear that wireless measurements in the hot side of the processes is of high interest. Therefore, the efforts in WP3 have been redirected to handle also this this challenge.

2.1 Concerned processes and parameters

Below is summarized data from D1.2 and conclusions from dialogues with the process owners regarding the hot side processes and their parameters that are of interest to measure.

2.1.1 Thermal grate

The primary parameters of interest in the thermal grate are the temperature on the grate, and the oxygen content of the gas within the grate. The required temperature range is 0° C to 1200° C, with oxygen content desired measurement range from 0 % to 100 %. Sampling rates of 1 Hz or less is sufficient, with accuracy requirement of 1-3 % for temperature measurements. The transit time through the grate is between 8 to 20 minutes, with only part of the time at maximum temperature. An important requirement for the thermal grate is that the gas flow in the system is to remain unimpaired by the sensors. To achieve this, a target sensor size of 10 cm diameter or less has been set. As further discussed below, it is believed that this will be enough to achieve the requirements for the grate, and to include within the scope of the project both parameters.

2.1.2 Blast furnace

For the blast furnace the requirements as listed by D1.2 are temperature, moisture, gas composition (oxygen content) and position. Here, the maximum temperature can reach 2200° C, and the throughput time for a sensor deployed in the process is several hours. Furthermore, the maximum diameter of a sensor is limited to 6 cm due to the access way to the process. This limitation makes it improbable that the device will be able to survive long enough to reach the bottom of the furnace. In dialogue with the process owners, the decision has been taken to primarily focus the sensor efforts on temperature and oxygen content, in order to achieve synergies with the thermal grate senors. The requirements for moisture and positioning will be revisited in the course of the project, in order to fully understand possible further development.

2.1.3 Walking beam furnace

Also in the walking beam furnace, the listed desired parameters are temperature, moisture, gas composition and position. The temperature requirement is similar to the thermal grate, with a maximum temperature of 1300° C. However, in contrast to the two processes listed above, the maximum allowed size is larger, up to 1 x 0.2 x 0.2 m. The transit time through the furnace is two hours, which together with the allowed size provides good opportunities for thermal protection and sensor survivability. Also for this process the decision has been taken to focus primarily on temperature and oxygen content.

2.2 Sensors

2.2.1 temperature sensors

The candidate technologies for implementing temperature measurements up to 1200° C were resistive temperature sensors (PT100 and similar), thermoelectric sensors, and sensors based on infrared emission of a hot surface. Although resistive sensors are favored for high accuracy temperature measurements at more modest temperatures, very few sensors are specified for operation above 650 °C, and no resistive sensors have been found to be specified for temperatures above 1000° C. On the other hand, thermoelectric sensors exist for temperatures well beyond the needs of this project. The industry standard material combination “Type K” is considered useable up to at least 1200°C, with thermocouple wires with insulation specified to well above this temperature readily available [1]. As this type of sensor is formed by welding wires of suitable materials together, the size and complexity of these sensors is minimal, simplifying the integration with the thermal isolation and the rest of the embedded Process Analyzer Technology (PAT). In addition, at this temperature the standard accuracy of a thermocouple appears to be comparable to that of the the closest PT100 candidate (about 10° C). Temperature measurements based on infrared emissions are in theory not limited to any upper temperature limit as the sensing element is not exposed to the temperature to be measured. The sensing elements are often specified to a maximum temperature of only 100° C [2] or less. However, they need a clear optical path between sensor and sensed surface. It appears that such a path would add greatly to the energy transport from surface to center of the thermal enclosure of a sensor package, and would additionally be difficult to manufacture.

From these options we find that thermoelectric sensors are the most attractive choice due to availability and ease of integration with the rest of the PAT. For initial tests we have selected to use the XC-K-20-50 cable from [1]. Such cable has a fairly typical cross-section area per conductor of about 0.52 mm^2. With a typical thermal conductivity of about 19 and 31 $Wm^{-1}K^{-1}$ ([3], [4]) of the two wires, the wires of such a sensor would conduct about 2.9 W at a temperature difference of 1100°C. This should be compared to an energy flow of about 180 W dissipated into a hollow sphere with an outer diameter of 8 cm and 70% hollow volume made from a high-quality insulating material [5]. A band-gap based integrated circuit sensor will be used as cold-junction reference for the thermocouple. This measurement can also be used for recording diagnostic information on the internal temperature rise of the sensor package.

2.2.2 oxygen senors

Oxygen concentration measurements remain a more challenging issue. The most commonly used high temperature oxygen sensor is the zirconium dioxide sensor used in automobiles for regulating the air/fuel mixture ratio. However, standard zirconium dioxide sensors (both so called narrow and wide-band types) respond to a difference in oxygen concentration, and would thus require a gas reservoir within the sensor with known oxygen concentration. This could be solvable, for example by using a small chamber with an oxygen absorbing material. We have located one type of zirconium dioxide based sensor that eliminates this by instead pumping oxygen back and forth to an enclosed chamber [6]. Although this sensor operates at an internal temperature

of 700°C, the documentation specifies a maximum gas temperature of 250°C. This could potentially be increased by reducing the heater supply current, but this would need to be investigated further. If not, the high heater power (6.8 W) could be a significant challenge to supply from small batteries that withstand 100 °C as required if the evaporation of water is used as the main internal thermal load.

Whereas zirconium dioxide sensors are based on measuring the electrical potential generated when oxygen is transported through a ceramic material, resistive oxygen sensors are also possible to build [7]. It appears that the only type of such sensor to reach commercial application is the titanium dioxide sensor commercialized by NGK-NTK for automotive (lambda sensor) applications. Such sensors appear to be strongly non-linear, but may nevertheless be worth investigating further. According to [8] the maximum temperature for such sensors is 850°C, but as these products are manufactured specifically for integration in automotive products, specifications for specific products does not appear to be readily available.

Electrochemical oxygen sensors are essentially metal-air batteries, typically using a consumable lead anode. All commercial sensors for oxygen concentration in gasses has a maximum temperature specification in the order of around 50°C, probably due to the use of a liquid electrolyte, requiring the internals of the sensor to be kept at a fairly low temperature. It would also require the ambient gas to be passed through channels and cooled before it reaches the sensor, greatly complicating the overall sensor design. While beyond the scope and time-frame of this project, it could be relevant to investigate the possibilities of building solid-electrolyte electrochemical oxygen sensors, as such sensors could potentially be used at significantly higher temperatures.

At the present it would appear that zirconium dioxide or titanium dioxide-based sensors are the most promising solutions for the present project, but due to power consumption and temperature limitations it may not be possible to implement oxygen concentration measurements in small sensor units and/or at the highest temperatures. For initial tests the KGZ10 sensor by Honeywell [6] appears to be the most promising candidate due to relatively high operating temperature and ease of use.

2.2.3 Position measurement

The position of the PAT at the time of data acquisition is of interest for all concerned hot side processes. One solution for accurately determining the position of a sensor within a process can be through measurements of the propagation delay of radio signals between the sensor and a number of fixed reference nodes. In order to minimize the influence of reflected waves bouncing off objects in the environment around the sensor it is desirable to use as wide bandwidth as possible, as this makes it possible to resolve the direct signal from indirect signals with small differences in path length. On the other hand, wide bandwidths has traditionally corresponded to very high operating frequencies (in order to keep the fractional bandwidth small). However, recent developments in RF circuits and standards has enabled so-called ultra-wideband (UWB) positioning based wide bandwidth transmission at moderate frequencies. For this project we intend to investigate if IEEE 802.15.4-2011 based solutions can be applied to position measurements in industrial processes. The basis for this work will be the Decawave DW1000 [9] chipset that uses 1 GHz bandwidth channels in the 3.5-6.5 GHz frequency band to achieve better than 10 cm positioning accuracy.

Another technology available for position determination is the use of low frequency magnetic field ”beacons”. The technique is based on measurement of the strength of the received magnetic in a transponder. One commercial use of the technology is to determine the position of wireless car keys in order to allow start of vehicle [10]. Another application is found in the tracking of elderly, disoriented people inside buildings. In these applications the target is not three dimensional positioning, but instead to determine if the transponder is in the vicinity of a single beacon, or, in between two.

Applied in Disire, we plan to use three beacons to transmit ranging pulses. The transponder will be equipped with a three dimensional receiver chip, that makes the reception omnidirectional

and independent on transponder orientation [11], [12]. The beacons will send at discrete time slots, with identification. At reception, the transponder measures the signal strength received by each beacon, and transmits the data back to overlying control system using traditional radio at 868 MHz or 2.4 GHz. Having data from three or more beacons will allow the determination of transponder position. The use of magnetic field holds the advantage that the magnetic field decays in a highly predictable manner in a relatively short distance from the antenna. This makes it suitable for the short range applications found in Disire. A challenge in the hot environment will be to protect the beacon antennas from excessive heat, either by insulation or by selection of heat resistant materials.

2.2.4 Moisture sensors

Zirconium dioxide sensors appear to be marketed for measuring both oxygen concentration and humidity [13], indicating a sensitivity to both gasses. On the other hand, thin film capacitive sensors are specific to water vapor but the maximum operating temperature found for a commercial sensor is 140°C [14]. Humidity measurements based on thermal conductivity does not seem suitable for high temperatures as the radiated heat transfer within the sensor would be substantial. A promising technique could be direct capacitive humidity measurement [15], but this solution does only appear to be available from one single manufacturer. Their sensors support up to 430°C, but they are quite large. While beyond the scope of this project, miniaturizing such sensors could be relevant to consider as future work. For this project the current conclusion is that thin-film capacitive sensors such as [14], used with pre-cooled gas (which will however limit the measurement range as the saturation water vapor concentration drops with temperature) is the most realistic solution if moisture measurements are essential.

Infrared gas analyzers enable compositions of multiple gasses simultaneously but are normally large and expensive devices. Potential could exist for miniaturizing such detectors to the point where they are feasible for medium-sized in-process sensors. Alternatively, emission spectroscopy using atmospheric pressure electric discharge may also offer potential for characterizing certain combinations of gasses [16].

2.3 Technical challenges

2.3.1 Temperature protection

One major technical challenge for the hot side wireless sensors is the extremely high temperatures in the surrounding environment. To keep the internal temperature of the PAT low for as long as possible, a thermal insulation need to be combined with the encapsulation of a material or fluid that will consume energy when heated inside the insulation. To find an upper bound on the feasible life-time of enclosed units a survey of commercially available insulating materials has been performed. Investigated materials include:

- Carbon black [17], survives very high temperatures (3000° C), thermal conductivity comparable to or better to the best solid materials found that support temperatures of 1200 C or more. A loose granular material that would need to be enclosed in some form of ceramic shell (typically alumina).
- Alumina fiber boards [18], useable up to about 1700° C, slightly higher thermal conductivity than carbon black, but comes in the form of rigid boards rather than a loose granular material.
- Moldable materials [19] that support up to 1260° C with a moderate increase in thermal conductivity exists.
- Microporous materials [20] exhibit far superior insulating properties, but withstand only up to about 950° C.

There is thus a clear trend that insulating materials that withstand higher temperature exhibit higher thermal conductivity at all temperatures. Some improvement could of course be achieved by combining materials, but as the thermal conductivity rises with temperature, thus requiring a significant fraction of the material before the temperature drops to the level that the next layer can support, the improvement is expected to be modest. Any insulating material will nevertheless transmit some energy. This energy is absorbed as temperature increase and/or phase change of the materials enclosed within the material. The following assumes that temperatures much higher than 100° C are not practical, especially as commercially available batteries appear to be limited to 125° C. Lower operating temperatures would extend the range of available batteries significantly. The most promising method of absorbing heat known to us at this point is the evaporation of water. This requires 2260 J/g. If one starts from ice (heat of fusion: 334 J/g) and the energy required for heating water 100° C, about 420 J/g, a total of about 3 kJ/g (or close to 3 KJ/cm^3) can be absorbed. Using the evaporation of water is however not without problems: Filling the core with ice/water would interfere significantly with antennas, and it could be challenging to ensure that the water only exits the core once it has evaporated, not in liquid form. For lower operating temperatures alcohols would be one alternative at the cost of significantly lower performance. For example, methanol boils at 65° C and absorbs about 1 KJ/cm^3 from 0° C to vapor at 1 Atm. All known solid-liquid phase changes are easier to use but perform worse still: Fatty acids such as Lauric acid has a heat of fusion of about 200 J/cm^3, and hydrated salts such as NaSO4-10H2O of about 350 J/cm^3. Further investigations into available salts may yield some improvements, but a relatively small compartment of water would nevertheless serve the same function as a significantly larger volume of any other known practically useable material.

For a given outer geometry, a trade-off exists between the thickness of the insulating material and the volume left for the material that absorbs the conducted heat. FEM simulations over a range of core and outer diameters show that for all materials relevant here, the optimum diameter for a core completely filling an insulating shell would be about 67% of the outer diameter, independently of the actual outer diameter. The resulting maximum operating time of three materials when the ambient temperature is 950° C is shown in Fig 1, with a corresponding plot for 1260° C shown in Fig 2. Thermal conductivity was interpolated at a constant level below the lowest temperature specified by the manufacturer and linearly above the highest temperature for “AX Moldable” where data was only available up to 800° C.

Initial prototype tests performed at MEFOS at the time of writing of this report indicate that the simulation results are achievable in real life. A sphere was fabricated of the Moldable material [19] with an outer diameter of 8 cm with the core filled with water soaked material. When subjected to an oven temperature of 1200° C the device held the core temperature at or below 103° C for 25 minutes. These and subsequent measurements will be further reported in future deliverables.

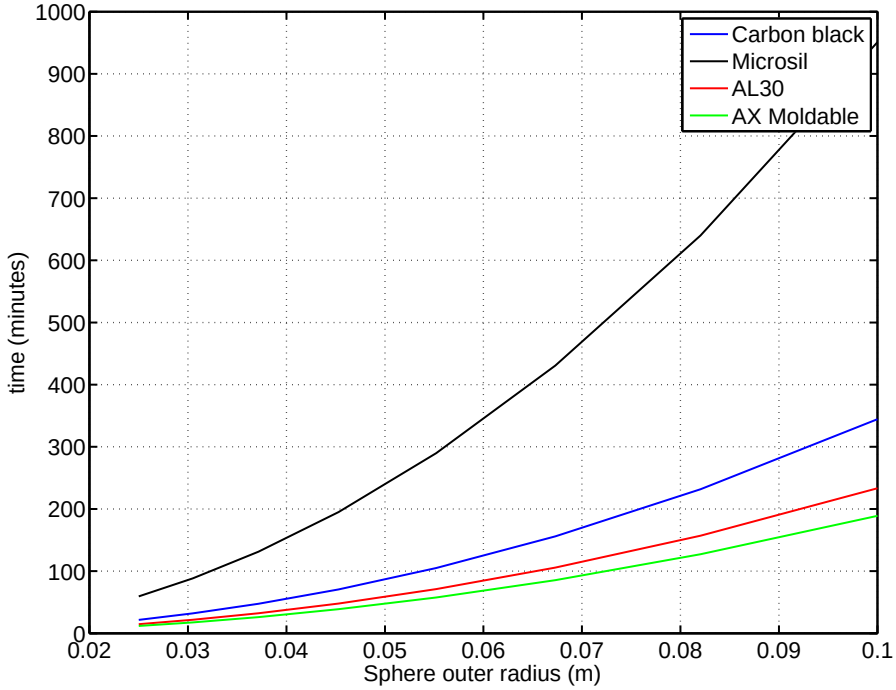

Figure 1: Operating time before core exceeds 100° C - ambient temperature 950° C.

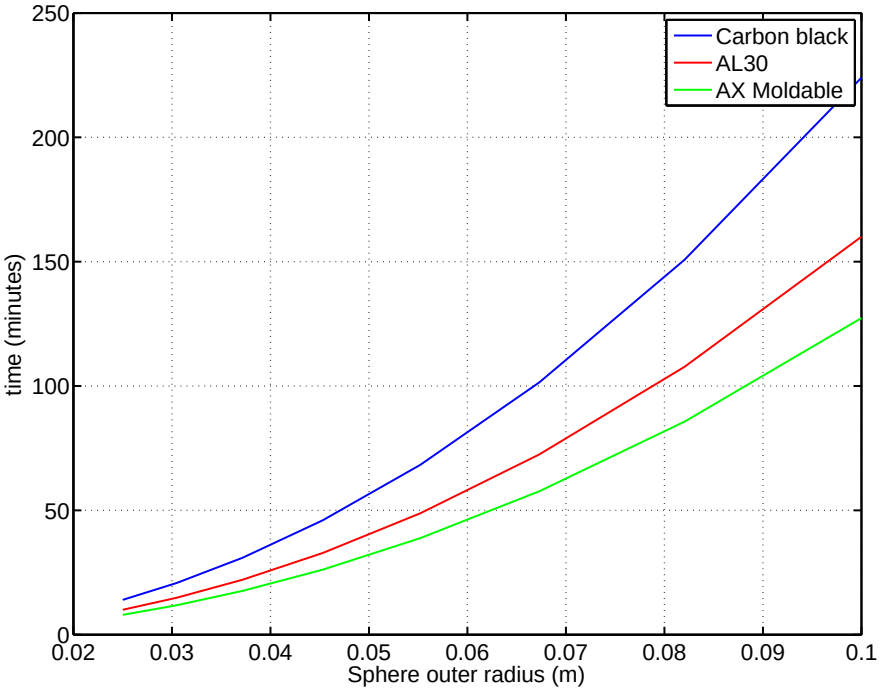

Figure 2: Operating time before core exceeds 100° C - ambient temperature 1250° C.

2.3.2 Radio environment

Although cold (dry and wet) sintered pellets has been shown to be fairly transparent at frequencies up to tens of MHz (see section 3.3.3) whereas unsintered pellets exhibit significant permeability (and at higher frequencies loss-tangents), the type of measurement setup used for these measurements limited the measurement to frequencies below 100 MHz. Because of the large size and difficulty of placing antennas in the processes of interest for this project, using significantly higher frequencies, and thus propagating waves rather than magnetic coupling, could be very beneficial. In addition, past tests only considered cold materials. At higher temperatures the conductivity of the material may increase substantially. In addition, the EBF uses coke in addition to the iron-ore pellets. Thus, experiments are being designed for characterizing the attenuation of heated granular materials. The current plan is to enclose miniaturized RF transmitters, transmitting either a modulated tone in the range of 100 MHz to 6 GHz, stepping through this range according to a predetermined schedule, or a square wave with harmonics over the same frequency range. These transmitters will be enclosed in thermal insulation, and measurements will be performed both with the sensor embedded in iron-ore pellets and/or coke at one or more temperatures. The signal from each set of conditions will be recorded using a suitable wide-band antenna placed outside the hot environment and digitized to characterize the attenuation affecting the signal, as well as recovering any data transmitted during the test (such as the internal or external temperature of the sensor).

3 Cold side wireless sensors

At the time of writing of the project proposal, a number of measurements with accompanied sensor development were envisaged for the cold side. However, as the project has evolved, the focus on measurements on the cold side has been reduced at the same time as the interest for the hot side has increased. Thus, the remaining target for cold side sensors is pure position, as further elaborated below.

3.1 Concerned processes and parameters

Below is summarized data from D1.2 and conclusions from dialogues with the process owners regarding the cold side processes and their parameters that are of interest to measure.

3.1.1 Positioning - non-ferrous mineral processing

For the non-ferrous mineral processing, the main identified need for positioning lies in the transportation of raw material from the origin in the mine, up to the point of crushing. Depending on the point of origin, the material will be put through different size selection processes. The background is that some parts of the mine contain hard rock, that needs to be processed in a manner different to soft material.

3.1.2 Positioning - ferrous mineral processing

One target for positioning in the ferrous mineral processing lies in the transportation chain for the finished product, the pellets. Here, the interest lies in the possibility to follow the product from the manufacturing onwards to the loading of a ship for delivery to customer. This gives knowledge of exactly which material batch is delivered to customer, and allows correct steering of material properties to be delivered.

Another targetis the determination of the position of a batch of material inside a large storage area, such as a silo. This would give knowledge of what material properties are to be expected not only at the moment of loading, but also what material properties that can be expected at a certain point in time in the process. Furthermore, for future use of in-situ sensors, the positioning allows the knowledge of where inside a storage area a certain measurement has been taken.

3.2 Sensors

3.2.1 RFID based transportation positioning

For positioning in a transportation chain, the choice of technology is passive RFID. In this technology, passive transponders use energy supplied by a reader antenna to power the internal electronics. The transponders are deposited in the material flow at the point of origin for the transforation chain to be measured. Detection of the transponders is made by the use of antennas around or over the process flow. Key advantages of passive RFID compared to active (battery powered) tags are low cost and unlimited shelf life. Conventional logistics applications such as tracking of packaged goods use ultra-high frequency (UHF) passive RFID to achieve long detection range. However, for detection through mineral products, water, and other materials exhibiting high attenuation at higher frequencies, the current trend is to use low frequency (LF) passive RFID. Known applications in mining industry have focused on mechanical robustness, and have used relatively large transponders to achieve acceptable detection rates. This however makes it difficult to ensure that the tags follow products such as iron ore pellets in a correct way.

As a part of research on tracking of granular products Kvarnström [21] investigated the read rate and residence time of RFID transponders of different sizes and densities. Significantly worse detection rate was observed for smaller, pellet sized transducers compared to larger (22mm)

transducers. This work also highlights the difficulties in ensuring that transducers larger than the bulk material follow the material accurately through silos. Wortley [22] used transponders from the SmartTag product line from Metso. While this work demonstrated the ability of such tags to survive through two crushing stages, this experiment also shows quite low detection rate for 20mm RFID tags. Rabe [23] showed low survival rate of custom made RFID tags in blasting applications, but did not investigate the probability of detection. While these and other works [24] demonstrate the significant academic and commercial interest in being able to track granular material flows, it is clear that the required tracking tools, e.g. RFID tags and systems need to be further investigated and developed.

3.2.2 Volumetric positioning

The technology foreseen to be used for volumetric positioning in the cold processes is the same as described in section 2.2.3 above.

3.3 Technical challenges

The use of RFID in the mining environment presents a number of challenges. These include readability due to long distances and unknown radio environment, uncertain orientation of transponders, mechanical and electrical interference, and separation due to size and density. The subsections below present conclusions and results on these technical challenges. The work performed in DISIRE on these matters link to work performed in the ePellet project, which was done by LTU in cooperation with LKAB. Thus, the sections below also contain results that were achieved in the frame of the ePellet project, as these to a high degree will affect the work and decisions taken in DISIRE.

3.3.1 Radio environment

This section summarizes the results from tests performed to investigate the electromagnetic environment at a conveyor belt transporting iron-ore pellets at “malmhamnen” in Luleå during early 2015. The tests were conducted at the location shown in Fig. 3, the belt going up to “siktfickan”.

Equipment As significant quantities of dust is produced when the band is transporting pellets a box (Fig. 4) was prepared for the measurement instruments. Pressurized air was forced into this box to provide cooling for the equipment and minimize the amount of dust entering the box during measurement with the belt running. The measurement box contained three main instruments:

- A **Rohde&Schwarz ESPI Test Receiver** used for measurements on the electromagnetic environment. It was switched between an EMCO 6512 loop antenna for the 50 kHz-30 MHz band and an AARONIA Hyperlog antenna for measurements between 800 MHz and 6 GHz.
- A **BOTEK B4200** 125 kHz RFID-reader provided by Electrotech. This reader was modified to enable measurement of the excitation and the resulting coil voltage. It was also modified by Electrotech to account for that the coil antennas have inductances different from what the reader was designed for.
- A **Ettus Research N210** digital sampler used for digitizing the output signals from the RFID-reader.

In addition, a portable magnetic field probe (Fig. 5) using the same type of 3D coil antennas intended for direction-insensitive pellet-size RFID-tags was built and used for measuring the magnetic field generated by the coil antenna.

Figure 3: The conveyor belt where the measurements were performed

Measurements Although two RFID-antennas were installed at the belt this report presents only results from the antenna surrounding the conveyor belt due to experimental difficulties and an unfavorably low signal level from the former. The following measurements were performed:

- Magnetic field strength at 10 positions along the length of the conveyor belt.
- Magnetic field strength at 9 positions over the belt, in the approximate volume where pellets can be expected.
- Responses from both large and small RFID tags were recorded using the digital sampler for 9 positions (only the large tags) within the volume where pellets can be expected. The response was detected in terms of the cross-correlation between the known response and the measured complex ratio between coil voltage and excitation (to suppress some of the noise in the excitation signal).
- Ambient magnetic field strength in the 50 kHz-30 MHz band and ambient electromagnetic field strength in the 800 MHz-6 GHz band. These measurements were performed both with the conveyor belt stationary and with the belt running without pellets.
- Modulation of the received signal due to motion of magnetic material or the antenna. This test was performed with the belt stationary, and in motion both with and without pellets.

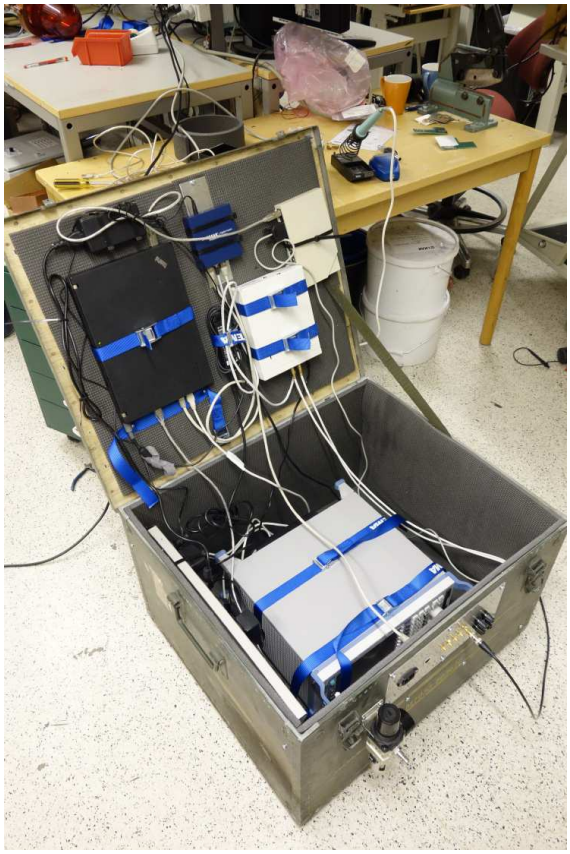

Figure 4: Measurement equipment in protective pressurized box.

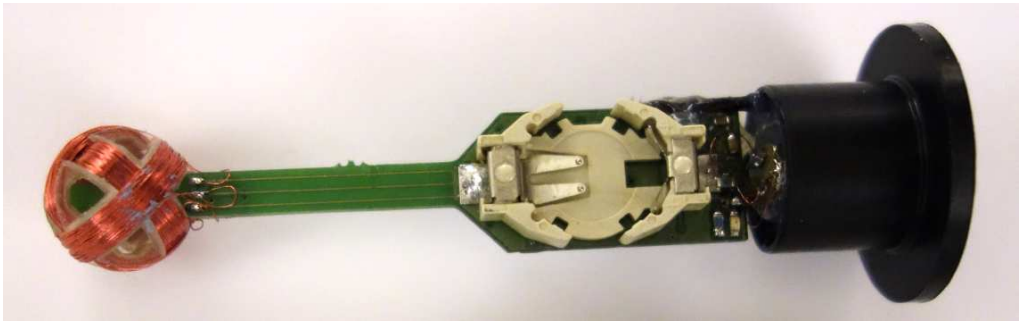

Figure 5: The 3-dimensional magnetic field probe used for measuring the magnetic field in the vicinity of the RFID antenna.

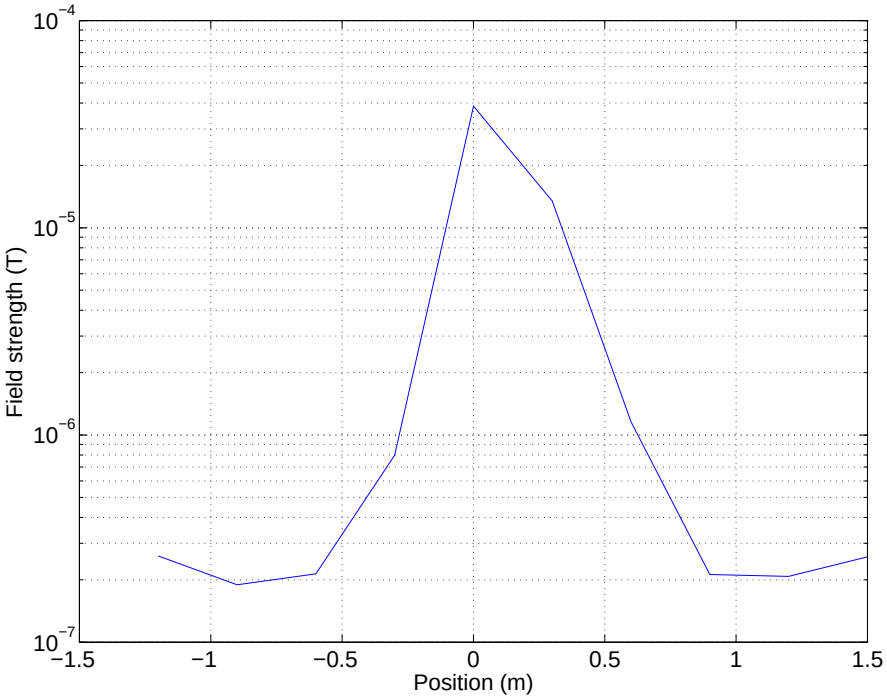

Figure 6: Total magnetic field measured along the length of the conveyor belt.

Results Both types of RFID tags were clearly detectable when detecting using the cross-correlation between one repetition of the response message. Tests with the large RFID tags showed an SNR (characterized as peak correlation to RMS correlation without tag) between 30.9 dB and 37.3 dB with an average of 33.5 dB. As the field was believed to be too weak to power the small tags only one test was performed at the position with the highest field. However, during post-processing this tag showed an SNR 18.1 dB which, especially if correlation to multiple repetitions of the message is used, could be sufficient for reliable detection. It should be noted that the duration of the messages from the small tags is twice as long as the large tags, adding 3 dB to the SNR. Both tags were aligned approximately along the direction of the magnetic field lines for maximum sensitivity. Thus, the number above represent the maximum signal levels that can be expected.

The total magnetic field measured along the length of the conveyor belt when the RFID antenna surrounding the belt was powered is shown in Fig. 6. Clearly the field generated with this antenna is highly localized long the length of the belt. Measurements in the volume inside the antenna showed more constant field strengths, ranging from a maximum field of 43 uT at the bottom corner of the belt to minimum value of 18 uT, with most recordings close to 20 uT.

The background electromagnetic (800 MHz-6 GHz) measurement showed no measurable signals except for the GSM-900 band. The result from the magnetic field measurements are shown in Fig. 7 and Fig. 8. The magnetic antenna factor, and thus background noise floor of the EMCO 6512 loop antenna used for this measurement decreases linearly with frequency up to a corner at about 5 MHz. Significant background magnetic fields are seen at 400-500 kHz and 1-3 MHz. It is also interesting to note that these fields changed significantly when the belt was in motion compared to when it was stationary, but it can not be ruled out that this change was due to some factor other than the state of the motors running this particular belt.

The spectrum of the ratio of the complex signals corresponding to the coil voltage and the

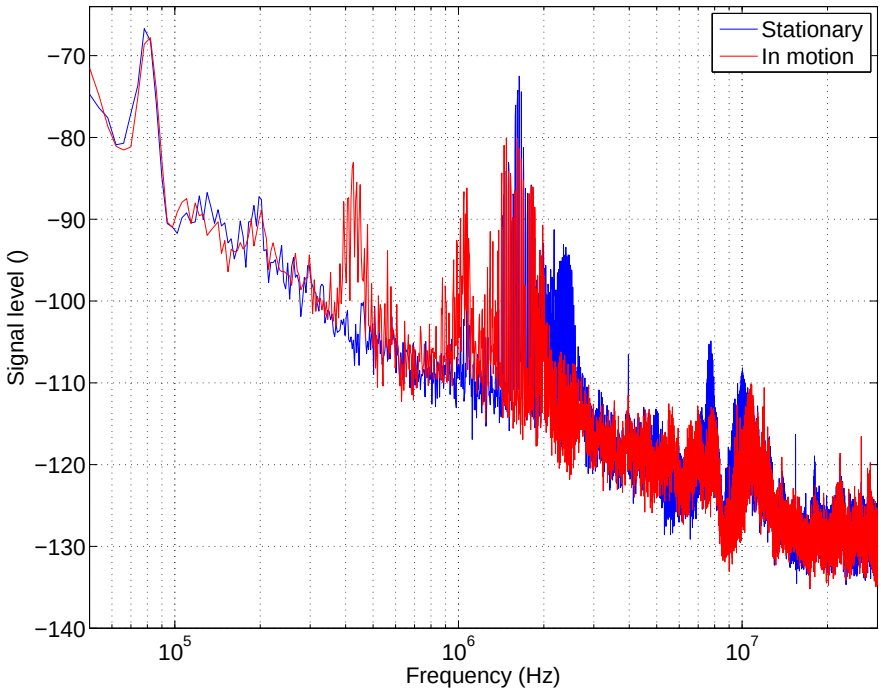

Figure 7: Magnetic field measured next to the RFID antenna.

excitation after digitalization and down-conversion is shown in Fig. 9. Clearly the motion of the belt modulates the signal, but the modulation decreases with increasing offset from the 125 kHz carrier frequency. The modulation when the belt was transporting pellets was significantly worse, indicating either that the effects of the slight permeability of the pellets is significant or that the larger mechanical load caused more significant movements of the belt or the antenna. Further measurements with more sensitive equipment would be required to gain quantitative measurements for offsets over 200 Hz. A second, more wide-band spectrum is shown Fig. 10 with the spectrum recorded with a tag in the reader coil shown as reference.

3.3.2 Vibration influence

It was believed that vibrations in the antenna would cause modulation that could interfere with actual signals. To invetsigate this matter, a laboratory measurement was performed in the framework of the ePellet project. In the experiment, an RFID reader (BOTEK B4200) and a 6x9 cm coil antenna supplied by ElectroTech was used for generating the powering magnetic field. The signal driving the coil and the voltage at the parallel resonant node were probed and connected to the inputs of a BasicRX board in an Ettus N200 digitizer. The sampled signal was decimated to a 195kHz bandwidth around 125 kHz and further processed using Matlab.

In order to simulate the effects of a vibrating antenna or vibrating conducting materials in the vicinity of the antenna an 18x22 cm aluminum plate was attached to a loudspeaker. The mechanical resonant frequency of the system of 170 Hz was used for subsequent tests. The plate was approximately 5 cm from the center of the coil antenna. The setup is shown in 11 and 12.

Figure 13 shows the average modulation spectra around 125 kHz without tag, with a tag close to the antenna and with the aluminum plate vibrating. This spectrum was calculated as the power

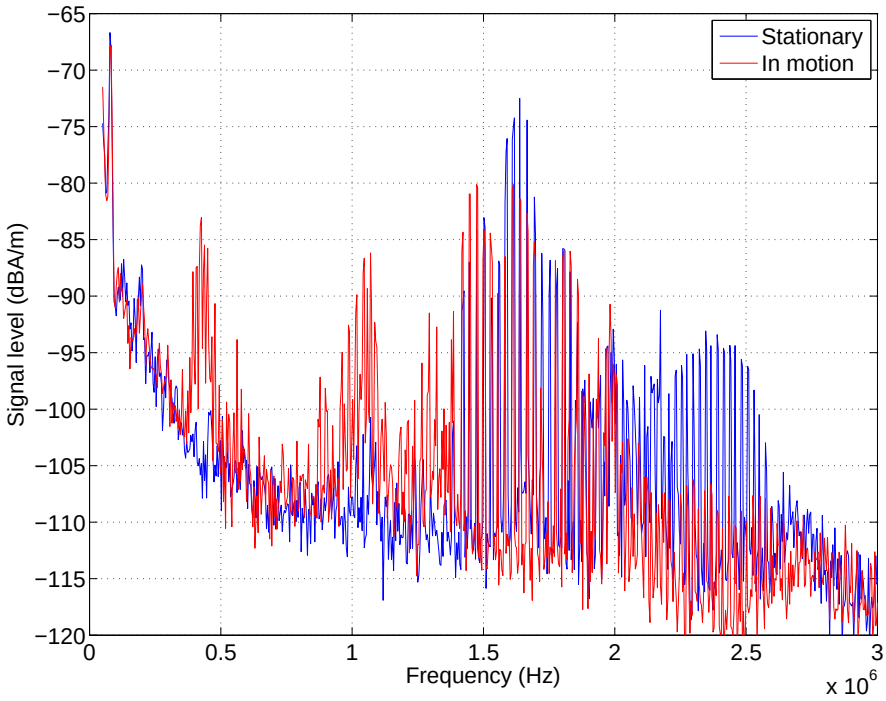

Figure 8: Zoomed view of the frequency range showing the greatest ambient magnetic field levels.

average of 100 fourier transforms of the ratio of the voltage at the parallel resonant node to the output voltage of the driver. It should be noted that while the plate was vibrating the detection range of the receive circuit of the reader decreased from about 7 cm to about 1 cm when using the tag shown in Fig. 14.

3.3.3 Magnetic properties of iron-ore pellets

The magnetic properties of the iron ore pellets was unknown at the onset of the ePellet project. Therefore, measurements were performed within the framework of the ePellet project to investigate these. One challenge in these measurement was to find a viable method of measurement. Using measurement methods developed for achieving high precision measurements when measuring on homogeneous materials may lead to skewed measurements if they are applied to granular materials unless the particle size is very small compared to the measurement cell. For example, one common method for measuring permeability is based on a coaxial cell shorted at one end. In this cell the magnetic field strength decreases with distance from the center conductor, and any voids in the material under test close to the center conductor will skew the measurement towards lower permeability. The classic method to manage this problem has been to simply make the measurement cell larger, but this becomes impractical when working with materials with large particle size.

For this work we attempted to find a measurement method better suited for coarsely granular materials. This is based on investigating different ways of keeping the material from coming in direct contact with the probe coil, and making the probe coil large enough that the field throughout the material remains fairly constant.

Possible geometries include (but is not limited to):

- A coil within a hollow within a spherical sample.

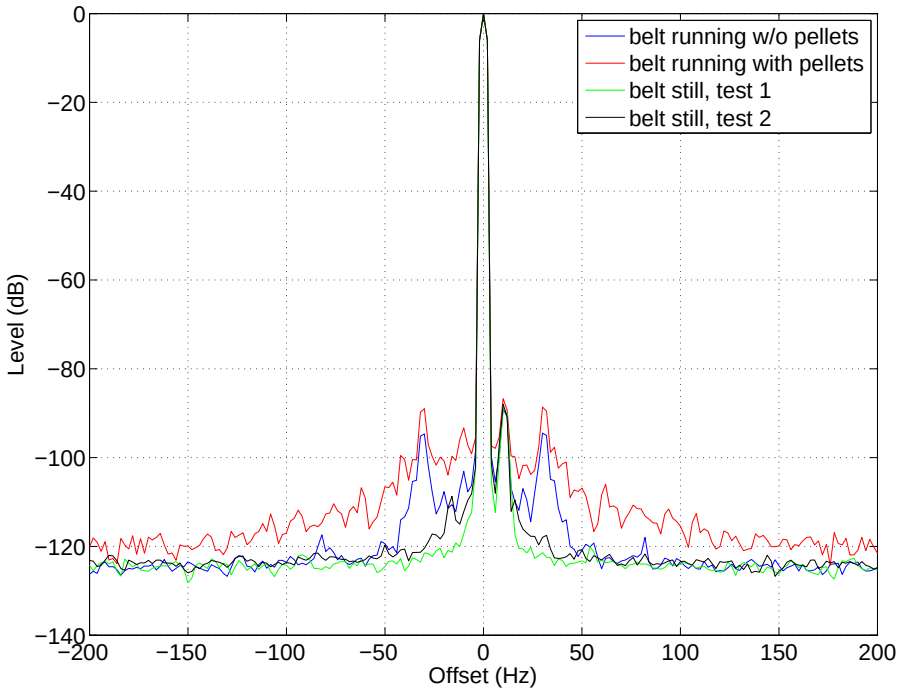

Figure 9: Received signal spectrum zoomed to the 200 Hz region

- A coil surrounding a sample (for example cylindrical or spherical) with some space between coil and sample
- A sphere within a pair of Helmholtz coils.

Based on it's mechanical simplicity we used the the second type of measurement in order to determine the properties of the materials relevant to this project (mainly sintered iron-ore pellets, but also un-sintered pellets are considered). Existing plastic bottles with simple geometry were used for defining the sample volume: D=9cm L=19.5cm, with rounded ends (r1=5mm r2=10mm). Measurements with and without sample within a probe coil were repeated 5 times. The sample permeability and loss-tangent shown below was found by comparing the measured coil impedance to hybrid MOM-FEM simulations with different values for μ and $tan(\delta_m)$ of the material.

As any inductance-based measurement this measurement will exhibit a low frequency limit due to the diminishing coil impedance for lower frequencies. The upper frequency limit results mainly from the increasing contributions of capacitance within the coil to the measured impedance. While the latter is in theory modeled in the electromagnetic simulations used for reference, the accuracy of the simulated model will not be sufficient to account for significant capacitive contributions. To experiment with extending the measurement range the measurement was performed using two different coils, one with a single turn of 2 mm copper wire, the other with 9 turns of 1.2 mm copper wire. Both coils had a diameter of 15.4cm. The electrical measurement was performed by connecting the coil as a shunt on a coaxial line between the ports of a R&Z ZVR vector network analyzer.

Measurements were performed on three samples: sintered dry pellets, sintered pellets wet with 5% water (by weight), and unsintered still moist pellets. Data for dry sintered and unsintered pellets are shown in Fig. 15 and Fig. 16, respectively. Wet sintered pellet was not measurably

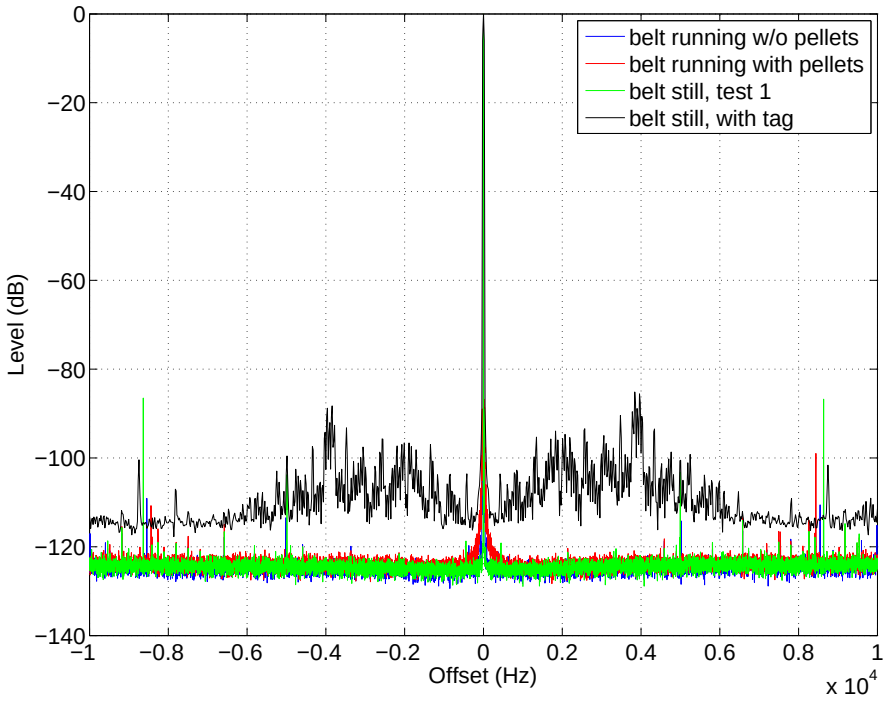

Figure 10: Wide-band received signal spectrum showing signal from a tag as reference.

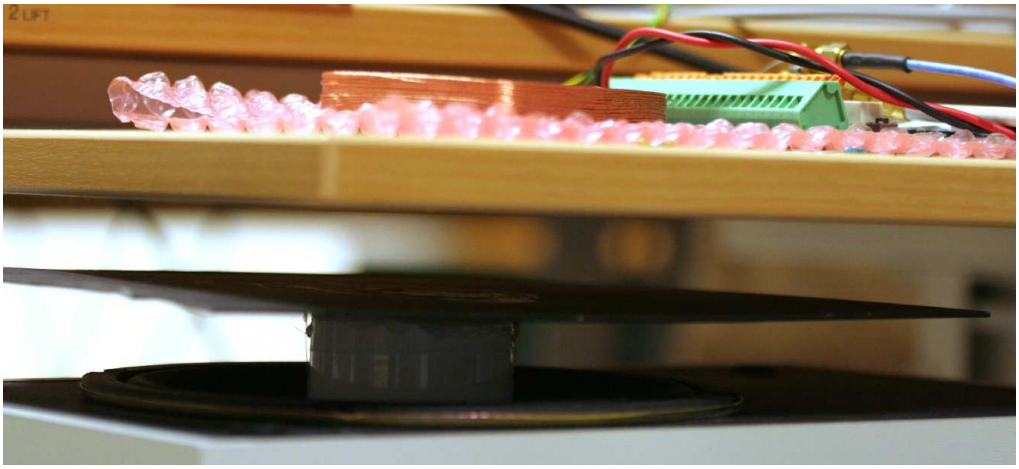

Figure 11: Vibration sensitivity test setup

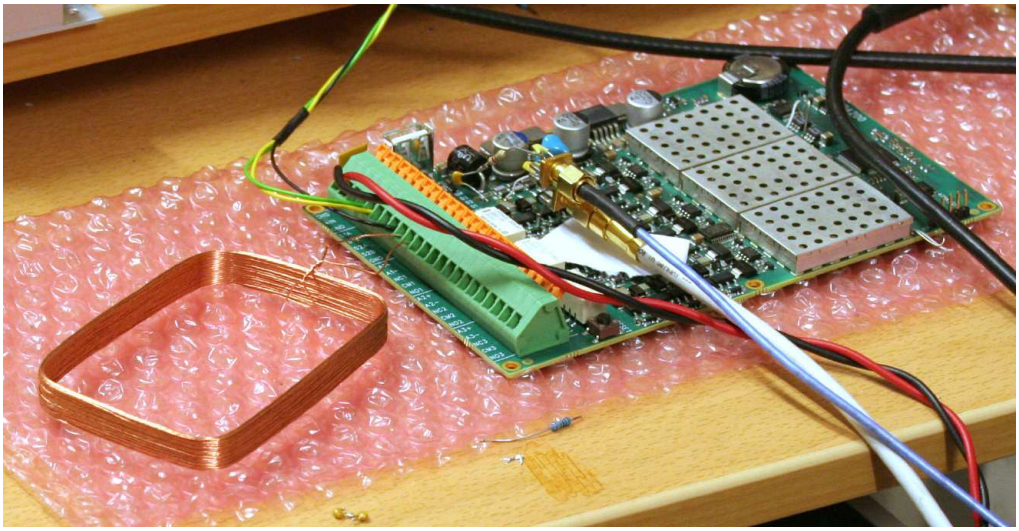

Figure 12: Vibration sensitivity test setup

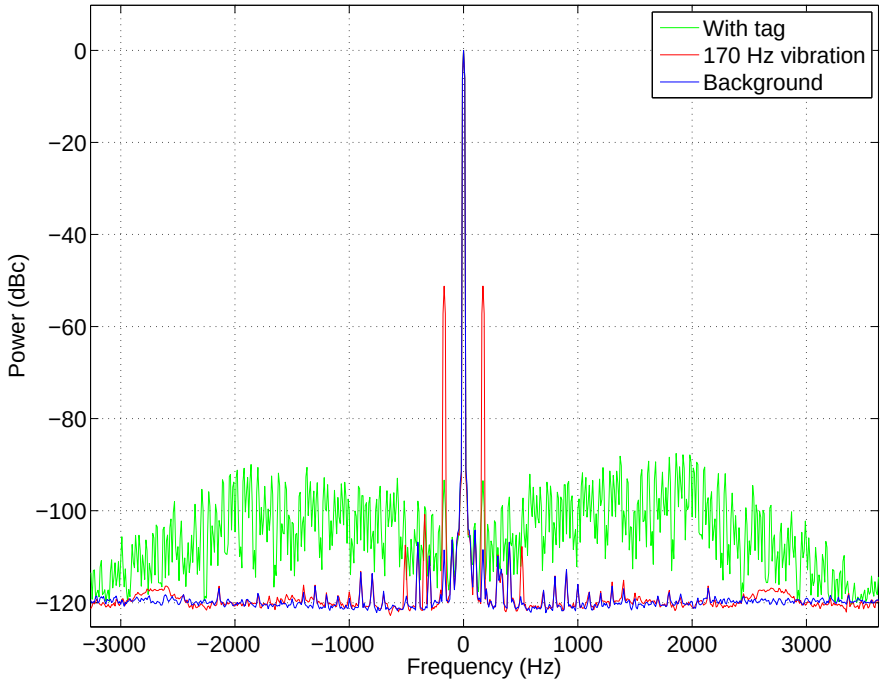

Figure 13: Measured modulation spectrum during vibration tests

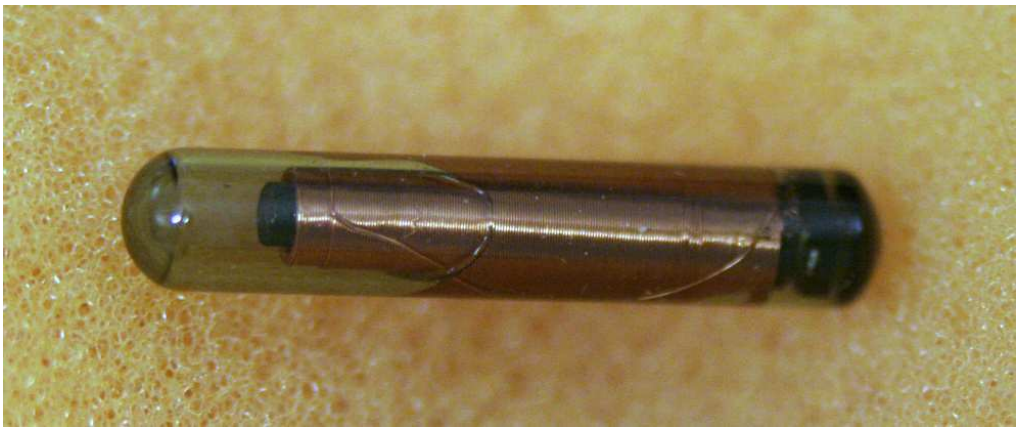

Figure 14: RFID Tag used for vibration measurements

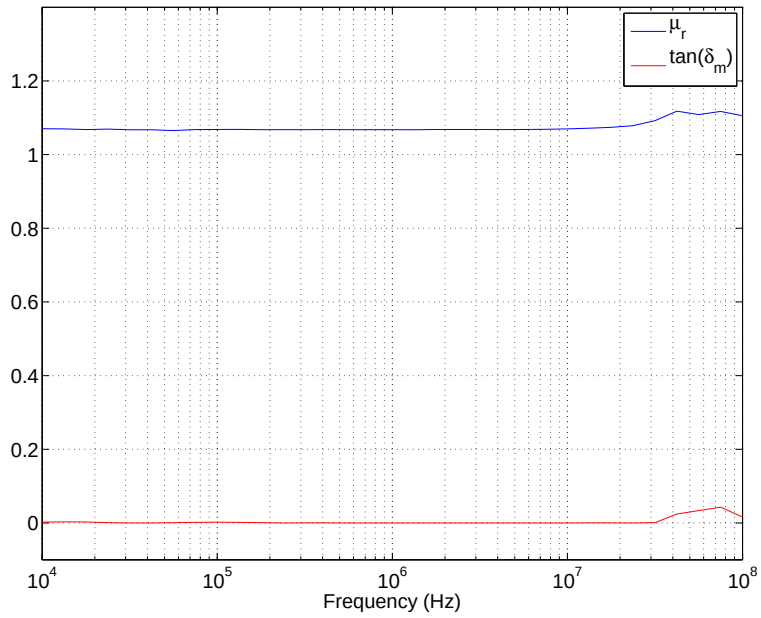

Figure 15: Permeability of sintered iron-ore pellets

different from their dry counterpart. The sintered pellets exhibited very constant permeability and a mostly negligible loss tangent over the whole 10 kHz-100 MHz measurement range. The slight increase at the upper end of the range may be an artifact of unmodeled parasitic effects becoming significant, and could be investigated further by repeating the measurement with a smaller coil. Unsintered pellets on the other hand exhibited a much more significant permeability of about 3 up to about 30 MHz, after which the permeability appears to fall while loss tangent rises significantly. This behavior is very similar to the that observed in ferromagnetic materials used for high-frequency transformer coils.

Fig. 17 shows the simulated signal attenuation from a 1 m coil to a 1 cm coil in a 1.4 cm hollow inside a 50 cm sphere of ferromagnetic and lossy material, normalized to the attenuation without material between the coils. Also shown is the calculated signal attenuation based on assuming

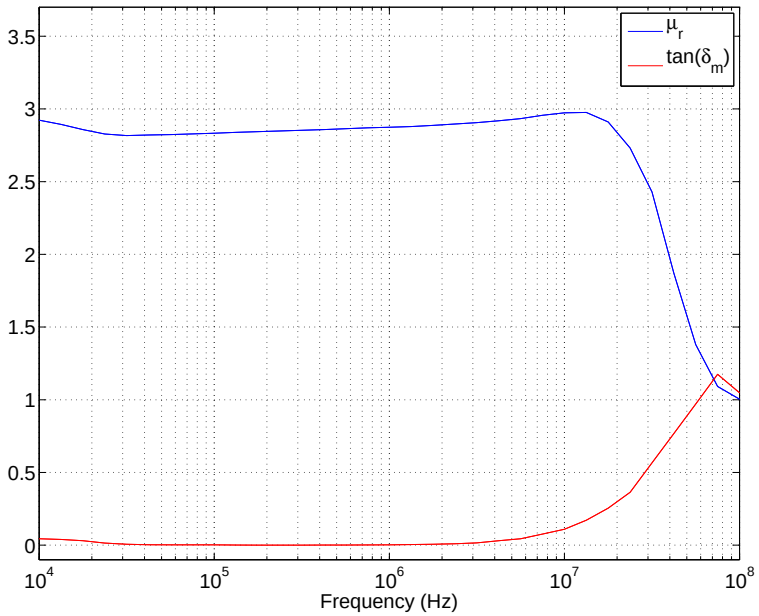

Figure 16: Permeability of unsintered iron-ore pellets

that the low reluctance of the magnetic material acts as a short circuit past the hollow where the coil resides if the reluctance of the air is adjusted by a factor 3.5 (justified by the fact that coil is close to the walls of the hollow rather than at the center of a wide narrow gap).

3.3.4 Antennas for ePellets

The small glass-encapsulated RFID tags that were used in earlier attempts at tracking iron-ore pellets fill only a small fraction of the volume available in the spherical volume of a pellet. Based on this it was assumed that significantly better antennas could be constructed simply by increasing the radius of the coil, perhaps even omitting the ferromagnetic core at a modest penalty. In total, 5 different coils were built and tested in the frame of the ePellet project, two of which are shown in Fig. 19 and 20. Measurement results for all 5 coils as well as from a commercial coil (Fig.18) are presented in Table 1 for a frequency of 125 kHz. Mutual coupling was measured relative to a 15.4 cm diameter loop, and available power is calculated with 1 A current driving this coil. It was interesting to find that coils 2 and 3 are only marginally better in terms of available power than the tiny coil 0. On the other hand, available power from coil 4 (with a ferrite core shaped to be comparable to an iron-ore pellet) is almost an order of magnitude higher than that of coil 0.

The conclusion from these experiments is that the increased complexity of the coil as well as the associated electronics in the design of a 3D RFID tag is not worth while. As the available power from a single dimension ferrite core coils is this much higher than the energy from an air-wound 3D coil, the ferrite coils will be visible with the same signal strength as a 3D coil for the majority of positions. Thus, dispensing a highr number of simpler tags seems to be beneficial.

3.3.5 Density considerations

Based on measurements on a set of 8 pellets an average density of 4.57 g/cm^3 was calculated. In order to achieve this density in RFID pellets where some use of less dense materials is expected, a significantly denser, preferably non-conductive, material that can be cast into suitable shapes

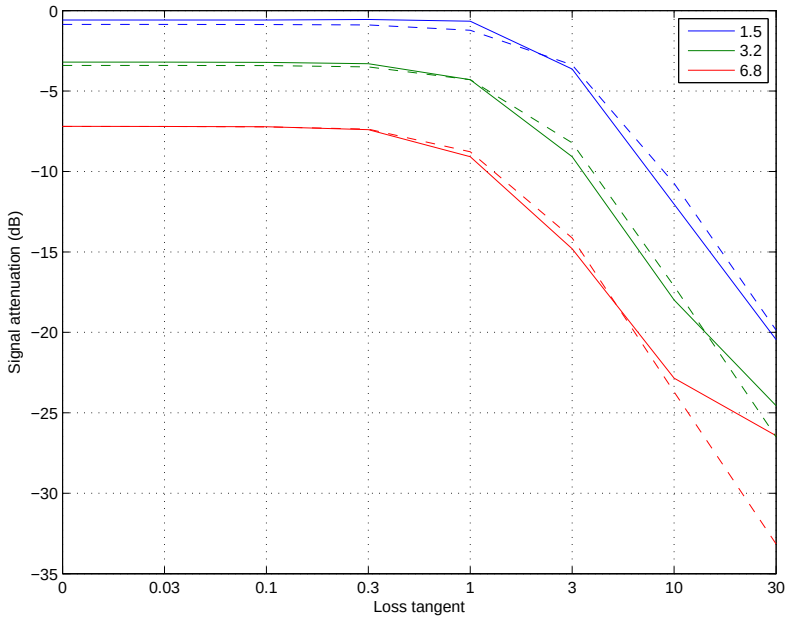

Figure 17: Normalized attenuation as a function of loss tangent, at three different permeabilities. Solid lines correspond to simulations whereas dashed lines are based on a magnetic circuit model.

Figure 18: Coil 0, the coil from a small commercial RFID tag.

Figure 19: Coil 2: second generation 3D coil, 50 μm wire, 800t.

Figure 20: Coil 4, wound on 11 mm ferrite sphere, 100 μm wire, 100t.

and used to fill voids in the assembled pellet would be useful. To this end an experiment with casting tungsten-filled epoxy was performed. While the mesh size of the available metal powder may have been smaller than optimal, the experiment nevertheless yielded a sample with a density of 7.4 g/cm^3. The density of EPCOS N87 ferrite (a reasonable material to use as a core) is specified as 4.85 g/cm^3. Thus, if the core constitutes a significant fraction of the pellet it could be difficult to achieve the correct average density.

Table 1: Inductance, mutual inductance to a 15.4 cm reference coil and maximum available power with 1 A flowing through reference coil. All measurements were performed at 125 kHz

Coil number	Description	Inductance	M	$M^2/4R$
0	From commercial tag	16.0 mH	3.1484 H	10.5 mW
1	3D v1 50 μm wire	236 μH	0.5457 H	2.0 mW
2	3D v2, 800t 50 μm wire	9.1 mH	4.3365 H	14.7 mW
3	3D v2, 220t 100 μm wire	650 μH	1.1315 H	12.1 mW
4	11mm ferrite sphere, 100t 100μm wire	540 μH	1.6391 H	101.8 mW
5	9.5mm ferrite sphere, 100t 100μm wire	475 μH	1.2184 H	64.0 mW

3.3.6 Electronics and reader for 13.56 MHz

To better understand which frequency bands are available for RFID applications and what field strengths are permitted in the respective bands, the relevant EU directive (2006/771/EG, updated a number of times, most recently with 2013/752/EU) was consulted. The bands associated with sufficient field strengths to be deemed relevant are summarized in Table 2.

It is interesting to note that the permissible field strength in the 13.56 MHz band has been increased from 42 dBμA/m to 60 dBμA/m specifically for RFID applications. Although much of the work hitherto made on the electronics for ePellets has been focused on 125 kHz, we foresee that a shift to the frequency band around 13.56 MHz would be beneficial. One strong reason for this can be found in that the permissible magnetic field power on that frequency is only 6 dB lower than on 125 kHz. This, combined with the fact that the frequency is around a factor of 100 higher, theoretically would allow for an induced voltage in an antenna to be 50 times higher at 13.56 MHz than on 125 kHz, which corresponds to a power increase of a factor of 2500. In addition, the higher frequency allows simpler antennas with lower inductance and thus lower number of turns. However, part of this improvement will be lost due to the, for a given antenna size, more efficient radiation of electromagnetic waves at higher operating frequencies. Since propagating waves are attenuated more slowly with distance compared to the magnetic field existing near and within the reader antenna, a specified permissible field strength at 10 m will correspond to a somewhat smaller magnetic field near the reader for readers operated at 13.56 MHz as compared to 125 kHz.

RFID at 13.56 MHz is commonly use in other applications such as smart cards, where a fairly complex signalling scheme is used. To allow for use in an industrial environment where limited time slots are available for communication, the signalling scheme and protocols will be investigated and adapted towards the needs of the DISIRE project. This could range from developing a tag-talks-first protocol for 13.56 MHz to schemes using pulsed transfer of power to the tag, and utilizing the quiet times for sending responses from the tags. This would eliminate the problem of distinguishing between the strong driven field and the weak responses from tags, as well as the problem of wide-band noise generated by the mechanical motion of the antenna or magnetic matierals in the vicinity of the antenna.

Efforts will be placed in the design of the on-tag analog electronics to achieve maximum efficiency in power transfer as well as in signalling. Also the reader technology at 13.56 MHz will be investigated and developed to optimize same parameters.

Table 2: Frequency bands where high field strengths are permissible for inductive applications or RFID specifically

Band (kHz)	Limit (dBμA/m at 10 m)
60.250-74.750	72
75.250-77.250	72
77.750-90	72
119-128.6	66
128.6-129.6	42
129.6-135	66
6765-6795	42
13553-13567	60
26957-27283	42

4 Fiber optical sensors

The fiber optic can be used as sensor, as we will see in this paragraph, as a novel approach to measure physical parameters in a reliable and effective way. Fiber-optic sensors are well suited for the measurement of a variety of physical quantities. Mechanical parameters like force, pressure, mass, path length, velocity, acceleration, rotation rate, vibration, flow rate, filling level, bending, and mechanical strain up to breakage, can be measured. There are sensors for measurement of electric and magnetic fields as well as fluorescence, concentration, ph-value, and furthermore temperature, humidity, refractive index, and sound. The use of fibers may provide a cost effective technology compared to other systems, since the fiber optic cable serves as the distributed sensory unit (replacing several conventional sensory units), while simultaneously it also provides the communication platform. The fiber optic based sensory system is easy to install, reliable, robust, resistive to environmental factors, maintenance-free, and provides long lifetime. These goals are achievable using two fiber optic technologies: single-point based on Fiber Bragg Grating and distributed sensors based on Rayleigh backscattering.

4.1 Advantages of fiber optic sensors

To understand the advantages of fiber optic sensing technique it is hereafter described with an example related with single point temperature measurement approach.

Small diameter Fiber Bragg Grating (FBG) temperature sensing is the ideal solution in any application where a high number of temperature sensing points must be installed over long distances and the application requires sensors of small sizes. In side by side comparisons with conventional thermocouples, the FBG is equally accurate, while providing for much faster response, wider operating range, no calibration, and less noise. The FBG temperature sensor is qualified for use in harsh environments and delivers the many advantages inherent to all FBG based sensors:

- Remote interrogation over large distances ($>$ 50km);
- Intrinsic long term stability;
- No electrical components used in sensing array and thus absence of any electrical signals;
- High reliability;
- Ability to withstand harsh environment thanks to intrinsic chemical stability of glass;
- Corrosion and water resistance;
- Intrinsic immunity to electric sparks and EMI/RFI;
- No risk of explosion due to short circuit;
- Easy cabling and resistant to fiber breakage (retro-reflection operating principle);
- High resolution, sensitivity and linearity;
- Small size and lightweight characteristics;
- No calibration required and long lifetime;
- Possibility of static and dynamic measurement;
- Cost-effective solution and low maintenance costs.

The cabling of fiber optic sensors to the Acquisition Device can be easily performed thanks to the high variety of reliable solutions already developed for telecom applications and by employing wavelength multiplexing. Moreover, low energy consumption of fiber systems allows the remote operation of the Digital Acquisition Unit (DAU) and digital data transmission. Standard FBG sensors with an acrylate or polyamide coating withstand respectively to temperatures up to 85° - 90° C and 170° - 180° C. Ormocer is a special coating employed in the Draw Tower grating technique and it allows to reach up to 200° C for short periods. High temperature single-ended FBG sensors are available on the market with special packaging to withstand at temperatures up to 250° - 270° C.

4.2 Concerned processes and parameters

These sensors are used in several sectors such as:

- Continuous lifetime health monitoring of bridges, dams, buildings, tunnels, ships, aircraft, trains, and other complex structures;
- Core building block for fiber optic transducers for strain, temperature, displacement, pressure, and acceleration;
- Measurement of absolute temperature on a structure´s surface;
- Measurement of relative temperature for compensation of strain measurements.

Main features making this technology appealing are:

- Fast response time;
- Qualified to same rigorous standards used for comparable electronic gages;
- Cable integrated with sensor package for fiber protection and strain relief;
- Fast, simple, repeatable installation;
- Connector protection fittings available for harsh environments;
- Armored fiber cable and rugged sensor package;
- Several package options for field and laboratory applications;
- Calibrated for high absolute accuracy.

Within the DISIRE scope several potential scenarios have been identified together with the DOW Chemical environment; some will be further analyzed, others, less promising, will be neglected:

- Temperature along the LPG header feeding the cracking furnaces (Promising scenario, to be further evaluated);
- Temperature of the naphtha header of the cracking furnaces (Promising scenario);
- Temperature of the distillation column (Promising scenario);
- Temperature profile along exothermic reactors (scenario with lower priority);
- Temperature of large compressors casing (scenario with lower priority).

4.2.1 Temperature along the LPG header feeding the cracking furnaces

To measure the temperature along the LPG header that supplies the furnaces may be very useful to troubleshoot and solve problems that DOW Chemical faces when LPG arrives to coil flowmeters in liquid phase. This situation leads to inaccurate reading that affects the furnace control and performance also in terms of energy efficiency. Thanks to the temperature measurement and recording along the feeding system, DOW Chemical could discern the source of the issue, such as insulation deficiency, insufficient heating capacity. This process deals with a temperature range $<50^{o}$ C, in line with FO sensor operative range.

4.2.2 Temperature of the naphtha header of the cracking furnaces

The temperature measurement along the naphtha header allows identifying and preventing potential early vaporization phenomena that could affect cracking furnace performance. This scenario is similar to the previous one with similar advantage in the control of the process and its performances. This process deals with a temperature range $<110^{o¨}$C, in line with FO sensor operative range.

4.2.3 Temperature of the distillation column

The availability of a detailed temperature profile of primary fractionator distillation column represents an added value for the control process and performance estimation. This process deals with a temperature range of 108^{o} - 200^{o} C, in line with FO sensor operative range. This possibility should be evaluated at consortium level since it deviates from description of activities. Nevertheless it is reported here because it should be an interesting application to be discussed even if at the moment is outside the scope of the project.

4.2.4 Temperature profile along exothermic reactors to identify ”hot spots”

The temperature measurement of the reactors means performance of the reactor functioning. In general exothermic reaction not properly controlled could turn out in explosion because of thermal runaway effects. This does not occur in the current DOW reactors, but an advanced temperature measurement system would bring to a better control of the chemical reactions. The fiber optic sensor could be used to measure the reactor temperature with a such density to allow the identification of hot spots that are difficult to be identified with current measurement system. This sensor application has been discussed at the beginning, but it’s implementation is not so promising as other solutions so it’s consideration has been degraded to lower levels.

4.2.5 Temperature of large compressors casing

The large compressors could suffer of fouling inside with related performance loss for that system and the whole related production linked to the system. The temperature of casing could help in identification of such issue. Furthermore the availability of a database of temperature evolution could be useful to investigate the fault prediction and condition based maintenance matter. This application have been discussed at the beginning while investigating feasible application of fiber optic sensors scenarios, later was considered as less important, so at this instance it has been abandoned.

4.3 Sensors

There are two principles that are used in fiber optic sensors: Fiber Bragg Gratings (FBG) used for single point measurement and Rayleigh backscattering used for distributed measures. Fiber Bragg Gratings (FBG) use UV-Laser light sent through an optic fiber to measure physical quantities such as temperature, forces, strain. The optic fiber is embedded or connected to the point

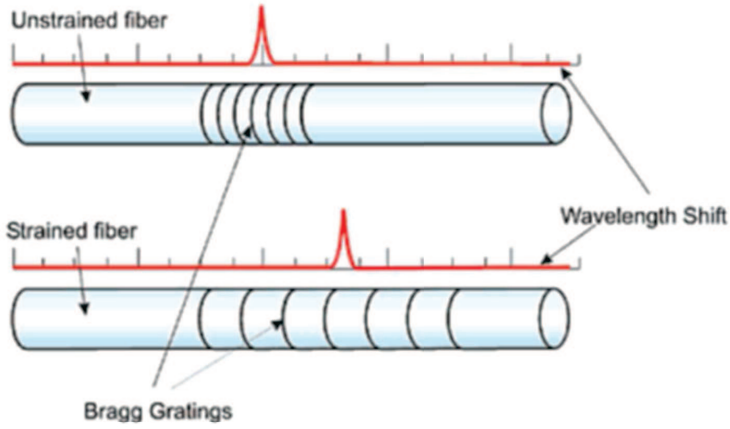

Figure 21: Fiber Bragg Gratings Principle.

of measure and once subjected to physical parameter variation, it elongate or compress. Under these circumstances, the laser is refracted from Bragg Gartings and differences in the measured index of refraction indicate the presence of a physical change like heating or deformation.

According to the requirements of the application, FBG sensors can be applied by the most suitable technique (embedded, on-surface sticking...) and with the required spatial distribution (a few sensors very close to each other or hundreds of sensors far away from each another). Thus a discrete sensing can be performed by connecting these sensors in series at any reciprocal distance in the body of one single optical fiber, providing a detailed (temperature-compensated) profile of the physical measure. Fiber optic cables can extend up to distances of several kilometers without suffering strong attenuation whereas electric cables with similar lengths present excessive attenuation. The distributed fiber optic sensors are based on Raman and Brillouin scattering. Both systems make use of a nonlinear interaction between the light and the silica material of which the fiber is made. If light at a known wavelength is launched into a fiber, a very small amount of it is scattered back at every point along the fiber itself. Besides the original wavelength (i.e. Rayleigh component), the scattered light contains components at wavelengths that are different form the original signal (i.e. Raman and Brillouin components). These shifted components contain information on the local properties of the fiber, in particular strain and temperature. Figure 2 shows the main scattered wavelengths components for a standard optical fiber. It can be noticed that the frequency position of the Brillouin peaks is dependent on the strain and temperature conditions that were present at the location along the fiber where the scattering occurred, while the intensity of the Raman peak is temperature dependent.

When light pulses are used to interrogate the fiber, it becomes possible, using a technique similar to RADAR, to discriminate different points along the sensing fiber by the different time-of-flight of the scattered light. Combining the radar technique and the spectral analysis of the returned light, it is possible to obtain the complete profile of strain or temperature along the fiber. Note that a fiber with a length of up to 30 km makes strain and temperature readings possible with a special resolution of one meter. This is a typical example of distributed sensing system. Raman scattering is the result of a nonlinear interaction between the light traveling in a fiber and silica. When an intense light signal is shined into the fiber, two frequency-shifted components called respectively Raman Stokes and Raman anti-Stokes will appear in the backscattered spectrum. The relative intensity of these two components depends on the local temperature of the fiber. Systems based on Raman scattering typically exhibit a temperature resolution of the order of 0.1°C and a spatial resolution of 1m over a measurement range up to 8 km.

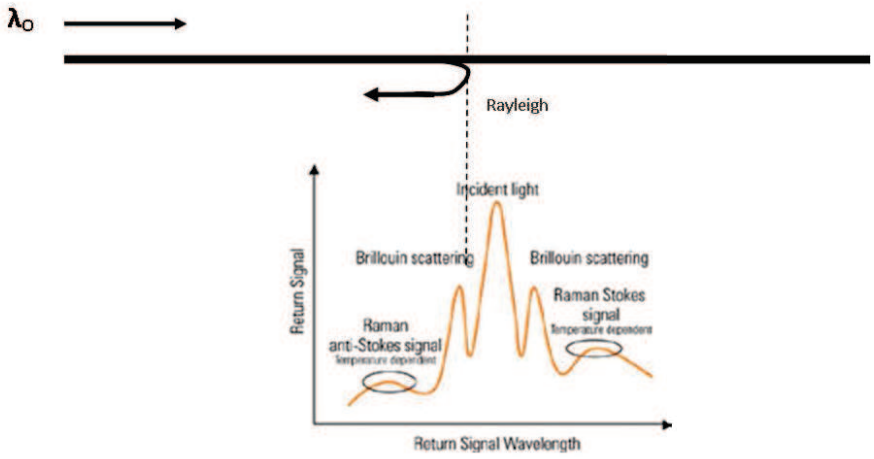

Figure 22: Light Scattering in an Optical Fiber.

4.4 Technical challenges

4.4.1 Use of the system in process outside the operative range

Although the temperature range of the fiber optics is wide enough to measure with success several industrial process, the furnace temperature are difficult to be managed. If the temperature is in the 1000° C magnitude order, the use of fiber optic sensors becomes tricky. Working in a range close to the boundary of operative condition should also create problems because there wouldn´t be enough dynamic to evaluate temperature changes. In such cases the temperature variations are measured thought an indirect measurement system. This kind of application is based on the thermal identification of the interface between the process under observation and the measurement system to estimate the temperature in a system observing its thermal exchange with the environment. For the furnace temperature estimation the sensor could be placed on the external casing; in this case has to be known the isolation characteristics of the container. At this stage of the project there´s a workgroup active in the definition of the cross correlation between the feasible acquiring system and the performances of the system. The fiber optic sensor technique is opening new possibilities that could lead to the possibility of better describe process performances to increase the whole efficiency. The final setup will be described in deliverable D8.1.

4.4.2 Cost

Considering that the setup is not defined yet the precise cost analysis will be done in future. As a preliminary estimation it is possible to say that, as depicted above, the fiber optic technology become cost effective, compared with thermocouples, when the number of sensing elements is over a breakeven that will be evaluated in final analyses.

5 References

References

[1] [Online]. Available: http://www.omega.com/pptst/XC_XS_XT_XL_WIRE.html

[2] [Online]. Available: http://www.amphenol-sensors.com/index.php?option=com_edocman&task=document.download&id=132

[3] [Online]. Available: http://www.goodfellowusa.com/A/T1-Thermocouple-Alloy.html

[4] [Online]. Available: http://www.goodfellowusa.com/A/T2-Thermocouple-Alloy.html

[5] [Online]. Available: http://www.zircarceramics.com/pages/rigidmaterials/specs/al30.htm

[6] [Online]. Available: http://sensing.honeywell.com/index.php/ci_id/50173/la_id/1/document/1/re_id/0

[7] R. Moos, N. Izu, F. Rettig, S. Reiß, W. Shin, and I. Matsubara, "Resistive oxygen gas sensors for harsh environments," *Sensors 2011*, 2011.

[8] [Online]. Available: https://www.ngk.de/en/products-technologies/lambda-sensors/lambda-sensor-technologies/titanium-dioxide-lambda-sensor/

[9] [Online]. Available: http://www.decawave.com/products/dw1000

[10] [Online]. Available: http://www.atmel.com/Images/article_optimizing_passive_keyless_entry.pdf

[11] [Online]. Available: http://www.ti.com/product/rf430f5978

[12] [Online]. Available: http://www.atmel.com/images/atmel-9124-lf-wake-up-demonstrator-atak5279-82_application-note.pdf

[13] [Online]. Available: https://www.yokogawa.com/an/download/manual/IM11M12A01-02E.pdf

[14] [Online]. Available: http://www.meas-spec.com/downloads/HTS2030SMD.pdf

[15] [Online]. Available: http://www.pronamicscontrol.com/Dewcon_Humidity_Sensor.pdf

[16] [Online]. Available: http://citeseerx.ist.psu.edu/viewdoc/download?doi=10.1.1.460.7880&rep=rep1&type=pdf

[17] [Online]. Available: http://www.cancarb.com/thermal-carbon-black/applications/hightemp.html

[18] [Online]. Available: http://www.zircarceramics.com/pages/rigidmaterials/specs/al30.htm

[19] [Online]. Available: http://www.zircarceramics.com/pages/moldables/specs/axmold.htm

[20] [Online]. Available: http://www.zircarceramics.com/pages/microporusinsulation/microporous.htm

[21] B. Kvarnström, "Traceability in continuous processes: applied to ore refinement processes," *Doctoral thesis, Luleå University of Technology*, 2011.

[22] M. Wortley, E. Nozawa, and K. Riihioja, "Metso smarttag - the next generation and beyond," *35TH APCOM SYMPOSIUM*, 2011.

[23] J. Rabe, P. Fouche, and K. O'Neill, "Development of a rf tracer for use in the mining and minerals processing industry," *The Third Southern African Conference on Base Metals*, 2005.

[24] W. Jansen, R. Morrison, M. Wortley, and T. Rivett, "Tracer-based mine-mill ore tracking via process hold-ups at northparkes mine," *Tenth Mill Operators' Conference, Adelaide, SA*, 2009.